



**The Abdus Salam
International Centre for Theoretical Physics**



2167-19

Advanced School on Direct and Inverse Problems of Seismology

27 September - 8 October, 2010

Receiver function techniques

Lev Vinnik
*Institute of Physics of the Earth
Moscow
Russia*

Receiver function techniques

Lecture notes by Lev Vinnik

Institute of Physics of the Earth, Moscow, Russia

1 Introduction

Most techniques for imaging subsurface structures, like seismic tomography, require a network of seismograph stations. Receiver functions are exceptions: they can be used with the data of a single station. The idea is to replace the network of stations by a network of seismic events. Seismic phases of body waves that are present in the seismogram can be classified into primary and secondary phases. For example, the primary P wave that arrives first is followed by secondary (reflected and converted) phases that are generated by this wave in the crust and mantle in the vicinity of the station. In order to detect the secondary phases in noise and to investigate the corresponding discontinuities, one should inspect a number of recordings of the same station. This is difficult, because source function of each event is usually different from the others, and the corresponding waveforms of secondary phases are different, as well. However, using a special kind of digital filtering (deconvolution), the primary waveform of each event can be transformed into a standard ‘spike’ or ‘bump’. The deconvolution transforms into a standard form every secondary phase, as well, and then they can be detected by stacking the deconvolved traces with appropriate time-shift (moveout) corrections. Receiver functions and similar techniques play an important role in the present-day global and regional studies of the interior of the Earth.

2 P receiver functions

The term “receiver function” was introduced for the radial component of the initial part of the seismogram $R(t)$ deconvolved by the vertical component $Z(t)$, where t is time. Instead of these two components, we can use L (or P) component corresponding to the principal motion direction of the P wave, and Q (or SV) component, perpendicular to L in the wave propagation plane (Figure 1). $Q(t)$ deconvolved by $L(t)$ can be termed receiver function, as well. For every discontinuity there are three secondary phases in the Q component, with comparable amplitudes (Figure 2): Ps (converted from P to S), $Ppps$ (transmitted as P , reflected from the free surface as P , and reflected from the discontinuity as S) and $Ppss$ (transmitted as S , reflected from the free surface as P , reflected from the discontinuity as S).

The multiple reflections of the higher order are much weaker and can be neglected. P_s , $Pppps$ and $Ppss$ are large in the Q component and missing in the L component. The only significant secondary phase in $L(t)$ is $Pppp$ (P once reflected from the free surface and once from the discontinuity), but usually this phase is much weaker than the parent P .

2.1 Deconvolution

Deconvolution can be performed either in time or frequency domain. Frequency domain deconvolution can be performed as follows. For the L and Q components, neglecting the instrument response, we can write in time domain

$$\begin{aligned} L(t) &= S(t), \\ Q(t) &= S(t) * E(t), \end{aligned}$$

Where $*$ denotes convolution, $S(t)$ is source function, and $E(t)$ can be written as

$$E(t) = \alpha_1 \delta(t - \tau_1) + \alpha_2 \delta(t - \tau_2) + \dots$$

Here α_i are amplitudes of the secondary phases, and τ_i are their delays relative to P . In frequency domain we can write

$$\begin{aligned} L(\omega) &= S(\omega), \\ Q(\omega) &= S(\omega)E(\omega), \\ E(\omega) &= H(\omega)/L(\omega). \end{aligned}$$

Dividing the spectrum of the Q component by the spectrum of the L component for extracting information on crustal structure is the essence of the spectral ratio technique, which was known prior to receiver function technique. The idea of the receiver function approach is to bring the spectral ratio in the time domain by inverse Fourier transformation. To avoid large errors caused by small values of the denominator, the spectral ratio to be Fourier transformed is modified as

$$E'(\omega) = \frac{Q(\omega)\overline{L(\omega)}}{\Phi(\omega)}G(\omega),$$

where

$$\Phi(\omega) = \max\{L(\omega)\overline{L(\omega)}, c \max[L(\omega)\overline{L(\omega)}]\}.$$

The bar over L denotes the complex conjugate, and $G(\omega) = \exp(-\omega^2/4a^2)$. Constant c is called ‘‘water level’’ and is selected empirically. $G(\omega)$ is required to suppress high frequencies and is also determined empirically. $E'(t)$ is recovered by inverse Fourier transformation.

The time domain deconvolution can be carried out as follows. Let the discrete representations of the actual P waveform and the desired waveform be s_k and z_k . The desired waveform is usually assumed to be δ -function: it is different from 0 only for a certain value of $k = K$.

$$\left. \begin{array}{l} s_k \text{ — seismic waveform} \\ z_k \text{ — desired waveform} \end{array} \right\} \quad k = 0, \pm 1, \pm 2, \dots$$

If the actual P waveform is filtered with the filter l_i , the resulting waveform is

$$v_k = \sum_{i=0}^{n-1} l_i s_{k-i}.$$

We are looking for the filter, which provides minimum difference $\min Q$ between the filtered and desired waveforms

$$\begin{aligned} \varepsilon_k &= v_k - z_k, \\ Q &= \sum_k \varepsilon_k^2. \end{aligned}$$

The coefficients of this filter satisfy the condition

$$\begin{aligned} \frac{\partial Q}{\partial l_j} &= 0, \quad j = 0, \pm 1, \pm 2, \dots, n-1, \\ \frac{\partial Q}{\partial l_i} &= 2 \sum_k \sum_{i=0}^{n-1} (l_i s_{k-i} s_{k-j} - z_k s_{k-j}). \end{aligned}$$

Here $C_{j-i}^s = \sum_k s_{k-i} s_{k-j}$ is autocorrelation of s and $R_j^{sz} = \sum_k z_k s_{k-j}$ is cross-correlation of z and s . This system can be written in the matrix form as

$$[C^s][L] = [R^{sz}].$$

Here $[L]$ is the column vector with elements l_i , $[R^{sz}]$ is the column vector with elements R_j , and $[C^s]$ is the matrix with elements C_{j-i}^s . It is assumed that the actual waveform consists of signal a and noise b

$$s_k = a_k + b_k.$$

We assume that the signal and noise are not correlated. Then matrix $[C^s]$ can be written as

$$[C^s] = \begin{bmatrix} c_0^a + c_0^b & c_1^a + c_1^b & \dots & c_{n-1}^a + c_{n-1}^b \\ c_1^a + c_1^b & c_0^a + c_0^b & \dots & c_{n-2}^a + c_{n-2}^b \\ \vdots & \vdots & & \vdots \\ c_{n-1}^a + c_{n-1}^b & c_{n-2}^a + c_{n-2}^b & \dots & c_0^a + c_0^b \end{bmatrix}$$

The elements of this matrix are autocorrelations of a and b . In practice, the noise is assumed to be white, which means that its autocorrelation differs from 0 only for diagonal elements of the matrix. The presence of noise is accounted for by presenting the diagonal elements in the form $c_0(1 + \lambda)$. The choice of this parameter, like waterlevel parameter, is arbitrary. When it is close to 0, the resulting spike is very sharp, but the inversion is unstable. When λ is large (say, 100), the deconvolved waveform is close to the autocorrelation function of the actual waveform. The optimum values are in the intermediate range. The deconvolution filter transforms the actual P waveform into “spike” or “bump”. In first approximation the transformed P waveforms are similar for different seismic events, and the same is true with respect to the waveforms of various secondary phases.

Instead of deconvolving every record separately, one can find a multichannel deconvolution filter for the set of records of many events. Single-channel deconvolution for continuous functions of time can be expressed as

$$v(t) = \int_{-\infty}^{+\infty} s(\tau)l(t - \tau) d\tau,$$

where $s(\tau)$ is the actual waveform, $l(\tau)$ is the deconvolution filter, $v(t)$ is close to the desired waveform. Multichannel deconvolution for N records is expressed as

$$v(t) = \sum_{i=0}^{N-1} \int_{-\infty}^{+\infty} s_i(\tau)l_i(t - \tau) d\tau.$$

In case of multichannel deconvolution, the filter for each record should be found by considering the other records. The calculations of multichannel deconvolution filter are in principle similar to the single-channel case, but require more algebra. The elements of $[C]$, $[L]$ and $[R]$ for multichannel deconvolution are matrices.

Figure 3 shows an example of multichannel deconvolution. In the left column there are three waveforms and their amplitude spectra. The dominant frequencies of the waveforms are strongly different. The results of single-channel and multichannel deconvolution of these waveforms with the same damping are shown in the middle and right column, respectively. The resulting spike in case of multichannel deconvolution is much sharper than in single-channel case. Multichannel deconvolution is superior to single-channel deconvolution if the amplitude spectra of the input waveforms are strongly different, like in the example in Figure 3.

In the literature there are descriptions of other methods of deconvolution.

2.2 Stacking P receiver functions with moveout corrections

To detect weak converted and reflected phases that are present in the receiver functions, one should stack receiver functions for many events. The delay of the converted phase relative to the parent P wave is given by

$$t(Ps) = \int_{r_d}^{r_0} \left(\sqrt{v_s^{-2} - p^2 r^{-2}} - \sqrt{v_p^{-2} - p^2 r^{-2}} \right) dr,$$

where p is ray parameter, r is the radial distance of the discontinuity, r_0 and r_d correspond to free surface and depth of conversion, v_p and v_s are P and S velocities. The time of the converted phase (its delay relative to P) is increasing with the increasing ray parameter value (or decreasing epicentral distance). For deep discontinuities the effect is large: the difference in travel time delays of the Ps phases from 660 km depth at epicentral distances around 30 and 90 degrees is close to 10 s. To detect the converted phase, the receiver functions should be stacked with moveout travel time corrections, which depend on the ray parameter (or epicentral distance) of event and the depth of the discontinuity. In practice the stack is calculated for many assumed depths of conversion. The real signals (the converted phases) are focused at depths, which are close to depths inferred from the travel times of these phases.

Contrary to the converted phases, multiply reflected phases have an opposite dependence of travel time on the ray parameter: the delay relative to P is increasing with increasing epicentral distance. In principle, for detecting the multiples one should calculate their theoretical delays and to introduce the moveout corrections in the same way, as it was made for the converted phases. Instead, one can apply slant stacking. The moveout corrections are calculated as a differential slowness (relative to P) multiplied by differential distance. This kind of stacking implies that the delay of the signal relative to P depends linearly on epicentral distance. Strictly speaking, this is not correct, but can be used as a first approximation. Then the converted and the multiply reflected phases can be detected in the negative and positive differential slowness range, respectively. Since slowness is proportional to wavenumber, stacking the receiver functions is very similar to the conventional wavenumber-frequency filtering with the receiver array. The properties of the wavenumber filter are determined by the distribution of the seismic events with epicentral distance in about the same way, as the performance of a receiver array depends on the array aperture. If the events are concentrated in a narrow distance range, this implies filtering with a poor resolution.

While the receiver function technique was initially developed for a single station, it can also be applied to seismic arrays. The individual receiver functions from different stations can be stacked with moveout corrections calculated for the same conversion point (piercing point), and the procedure can be repeated for all possible piercing points. Calculations of the moveout corrections require ray tracing in the appropriate velocity model. For a linear array, amplitude of the stack is presented as a function of time after P (or depth) and of the horizontal coordinate. This is the essence of the common conversion point (CCP) method. Sometimes this method is incorrectly referred as "migration". The true migration is based on stacking the receiver functions for neighboring scattering points with appropriate weights and move-out corrections. This method has much in common with migration used in seismic exploration. While in the theory migration is superior relative to CCP, in practice the results obtained so far are comparable in resolution. Both techniques may have problems with distinguishing between the true converted phases and multiple reflections (reverberations).

Signal/noise ratio enhancement by stacking depends on the degree of correlation between the signals in the individual traces. The effect of scatter in the traveltimes is quantified with the expression:

$$E/E_0 = 1/n + [(n - 1)/n] \exp(-\sigma^2\omega^2),$$

where E is the actual energy in the stack, E_0 is the maximum possible energy, n is the number of stacked traces, ω is angular frequency of the signal, and σ is the rms value of the traveltimes fluctuations. There are examples of detection of phases with a frequency of 1 Hz. Such observations are only possible if σ is not much larger than 0.1 s.

While stacking of the receiver functions is essentially a linear procedure, there are nonlinear detection techniques, like N -th root method. Instead of the initial trace, the N -th root of it with the sign preserved is taken, and the transformed

traces are stacked:

$$E_N(t) = \frac{1}{M} \sum_{i=1}^M |l_i(t)|^{1/N} \text{sign}\{l_i(t)\}.$$

The stack is raised to the N -th power, with the sign preserved

$$E'_N(t) = |E_N(t)|^N \text{sign}\{E_N(t)\}.$$

There are examples when application of this method leads to a significant improvement of the signal/noise ratio. This method distorts waveforms, but the distortion is minimal for $N=2$.

2.3 Inverse problem for P receiver function

The secondary phases, which are present in receiver function, have different sensitivities to the properties of subsurface structure. Multiply reflected phases are sensitive to both velocity and density contrasts at the discontinuities. If the width of the discontinuity exceeds quarter of the wavelength, the reflection coefficient becomes very small. The converted phases are strongly sensitive to the S velocity contrast. Sensitivity to the P velocity contrast is lower. The transmission coefficient of the converted phase is reduced significantly relative to the maximum value, if the width of the discontinuity is around the S wavelength or larger.

Inverse problem for receiver functions was approached in several studies dealing mainly with crustal structures. The best way of inverting receiver functions would be to separate and investigate all secondary (reflected and converted) phases. This, however, is usually difficult, because they interfere with each other, and their differences in slowness are small. Therefore, generally, the wavefield should be interpreted without separating the constituent phases. Useful results can be obtained for plane-layered models, whereas practical methods for more complicated structures may appear in the future. At high frequencies (around 1 Hz), the wavefield is dominated by randomly scattered rather than reflected and converted phases, and the technique is applicable starting from about 0.5 Hz. In the algorithm developed in the IPE (Moscow), the synthetic Q component is calculated by using the expression

$$Q_{\text{syn}}(t, v(d), c) = \frac{1}{2\pi} \int_{-\infty}^{+\infty} \frac{H_Q(\omega, v(d), c)}{H_L(\omega, v(d), c)} L(\omega) \exp(i\omega t) d\omega,$$

where $v(d)$ is a vector of the variable model parameters, c is the apparent velocity, $H_Q(\omega, v(d), c)$ and $H_L(\omega, v(d), c)$ are the SV and L components of the theoretical frequency response of the layered structure, and $L(\omega)$ is the spectrum of the stack of deconvolved L components. The theoretical response is computed using Thomson-Haskell matrix method. To test the model, the synthetic SV component is compared with the stack of the receiver functions. The inversion procedure is based on the general method of solving ill-posed inverse problems. The optimum parameters of the model can be found by iterative minimization of the smoothing functional:

$$F(v(d), c) = \|SV_{\text{obs}}(t) - SV_{\text{syn}}(t, v(d), c)\| + \alpha q(d) \|v(d) - v_0(d)\|,$$

where $v_0(d)$ is the starting velocity model, $q(d)$ is the weight functions and α is the damping parameter. The parameter α changes during the inversion procedure as $\alpha_{p+1} = \alpha_p \Delta\alpha$, where α_p is the value of α in the preceding iteration, and $\Delta\alpha$ is less than 1.0. The second term of this expression keeps the solution near the starting model.

The models generated from gradient-based methods of optimization usually depend on the starting models, because the error surface has several local minima. There are other methods that make a search for the global minimum. In particular, Simulated Annealing algorithm belongs to the group of directed Monte Carlo methods that explore a wide space of possible solutions more efficiently than do pure Monte Carlo random search techniques. The algorithm deals with a series of models produced by random walk. The misfit between the observed and theoretical data converges to the global minimum independently of the starting model, if the series of misfits obeys the Metropolis rule. This rule is formulated in terms of a parameter termed "temperature". In the theory, a convergence to the global minimum is only guaranteed, if, during the search, the temperature decreases indefinitely slowly, and the number of moves tends to infinity. In practice, temperature schedule is an essential problem of application of the SA techniques. In most cases, the "best" model corresponding to the global minimum is not so important as the whole ensemble of acceptable models, that can be obtained with this technique. SA algorithm was applied to a number of geophysical problems, including the inversion of the receiver functions.

The highest accuracy of the inversion is achieved in the high gradient zones, because these zones produce the converted phases, and the solution appears to be well constrained. Therefore, the best results are usually obtained for the upper and the lower crust, but not for the middle crust with a nearly constant velocity. There is a trade-off between the average velocity above the discontinuity and its depth. The uncertainty can be reduced by using receiver functions jointly with surface wave dispersion curves.

3 S receiver functions

The major shortcoming of P wave receiver functions that were discussed in the preceding sections is the difficulty of separating the phases converted at deep discontinuities from multiples reflected or scattered at shallow discontinuities. Ideally, the converted phases and multiples that arrive in the same time interval have different apparent velocities, but this difference is negligible for the converted phases from discontinuities in the crust and the uppermost mantle. This problem can be solved with the S wave receiver function technique, which is based on the observations of Sp (S to P converted) phases. Sp phases from discontinuities in the mantle arrive earlier than the crustal multiples, and hence are easily distinguished from them.

To detect the Sp phases, the 3-component seismogram is decomposed into P , SV , T and M components. The SV axis corresponds to the principal S particle motion direction in the wave propagation plane. The P axis is perpendicular to the SV in

the same plane and is optimal for detecting Sp phases. The T axis is perpendicular to SV and P . The M axis corresponds to the principal motion direction of the S wave in the $T - SV$ plane and is characterized by the angle θ with the SV axis. The P components of many records of the same station are deconvolved by their respective M components. Combined processing of the deconvolved P components yields $P_c(t)$ and $P_s(t)$, where t is time, $P_c(t)$ is the P component (observed at the free surface) corresponding to the incident SV and deconvolved by the SV recorded at the free surface. The expression for $P_s(t)$ includes a similar term for SH and two other terms. Excitation of $P_s(t)$ is possible in anisotropic medium.

The unknowns $P_c(t)$ and $P_s(t)$ are obtained by minimizing the misfit E between the observed and predicted P components:

$$E(t) = \sum_{i=1}^N w_i^2 [P_i(t) - P_c(t)\cos\Delta\theta_i - P_s(t)\sin\Delta\theta_i]^2,$$

where $P_i(t)$ is the P component of event (i) deconvolved by the M component of the S wave, $w_i^2 = 1/\sigma_i^2$, and σ_i^2 is the variance of noise in the i -th record. The solution for either $P_c(t)$ or $P_s(t)$ is equivalent to stacking of $P_i(t)$ with weights depending on their respective θ and σ_i^2 . The procedure of record processing involves evaluation of the standard error of the amplitude of the stack. To account for the difference in slowness between the Sp phases and the parent phases, the estimates of P_c and P_s are obtained by stacking the deconvolved P components with move-out time corrections.

The most efficient way of using S receiver functions is joint inversion with P receiver functions. Our technology of joint inversion was described and used in the studies of the Tien Shan, Indian shield, Himalaya and other regions. To generate synthetic receiver functions and compare them with the actual receiver functions we use the Thomson-Haskell matrix algorithm for plane waves and plane layers, with Earth flattening transformation. We conduct a search for the optimum models by using an iterative method, similar to Simulated Annealing, from 4 randomly selected starting points. For each starting point we test up to 100000 models until they converge to those which provide a small misfit between the synthetics and the actual receiver functions. The depth range is usually up to 300 km. The trial models consist of 4 layers in the crust and 5 layers in the mantle. The non-uniqueness of the joint inversion of P and S can be further reduced by using teleseismic S and P travel-time residuals. The residuals can be inferred from the travel times of the Ps phases from the 410-km and 660-km discontinuities.

Our experience shows that that the P and S receiver functions are complementary, and their joint inversion is more robust and informative than separate inversion. In particular, calculations of the receiver functions involve measurements of the apparent angles of incidence of the P and SV waves, and these angles are used as an input in the inversion procedure. It can be shown that the angle of incidence of the P wave depends only on the S velocity, whereas the angle of incidence of the S wave depends on both P and S velocity. Therefore the two angles, if used jointly, constrain both velocities and the Vp/Vs ratio. The Vp/Vs ratio is also constrained by the transmission coefficients of the Ps and Sp phases, the travel-times of crustal

and upper-mantle multiples in the P receiver functions and by P and S traveltime residuals. The V_p/V_s ratio is either difficult or impossible to obtain by other means.

4 Other kinds of receiver functions

There are other seismic techniques with a very similar approach to the data treatment. For example, studies of the mantle discontinuities, which are based on observations of precursors to SS , use a similar technique. Teleseismic SS phase (S wave reflected from the Earth's surface in the midpoint between the source and the receiver) is preceded by weak phases (precursors), which are reflected (or scattered) from the underside of the mantle discontinuities. In this case the parent phase is SS , and SH component of the record is deconvolved by the SH component of SS . The deconvolved records of many events at many stations with the bouncing points within certain regions are stacked. The times of the precursors relative to SS depend on the S velocity in the mantle and depths of the discontinuities. With this technique, the depths of the major mantle discontinuities (those at about 410 km and 660 km depths) were mapped worldwide. However, the accuracy of these estimates is disputable.

A similar approach was used in the analysis of multiple ScS reverberation. The coefficients of reflection of SH from the Earth's surface and the core-mantle boundary are close to unity, and the recordings of strong deep events contain a sequence of clearly visible waves reflected a few times from the free surface and the core-mantle boundary. Weaker phases, reflected from the mantle discontinuities accompany these strong ones. To detect the phases reflected from the mantle discontinuities, recordings of many events are deconvolved by ScS and the deconvolved traces are stacked with appropriate moveout corrections.

The best data on discontinuities in subduction zones are provided by observations of phases, which are converted from S to P in the source region and arrive in the tail of the P wave. In short-period frequency range these phases sometimes are detected in array recordings of deep events. Now, the receiver function technique is extended for detecting these phases in the broadband recordings of conventional seismograph stations. The idea is to deconvolve the vertical component of the teleseismic record by the S waveform in the same record and to stack the deconvolved vertical components of many records. This technique has been used in the search for discontinuities in the lower mantle.

5 Receiver functions for anisotropic media

In the isotropic, laterally homogeneous medium the P wave is coupled only with SV . In anisotropic medium, all three components of motion (vertical Z , radial R and transverse T) are coupled.

One of the most useful techniques for measuring azimuthal anisotropy in the mantle is closely related to the receiver function technique. In azimuthally anisotropic

medium, S wave with a nearly vertical direction of propagation splits into two quasi-shear waves, which propagate with different velocities, and polarizations of which are perpendicular to the wave propagation direction and to each other. Assume that on its way to the Earth's surface the S wave propagates through an anisotropic layer. Neglecting the vertical component, the relationship between the radial (R) and transverse (T) components of this wave above the layer and its SV and SH components beneath the layer can be described in frequency domain by matrix equation

$$[A(\omega)] = [F(\omega)][S(\omega)],$$

where $[A(\omega)]$ is column vector with the elements $R(\omega)$ and $T(\omega)$; $[S(\omega)]$ is column vector with elements $SV_0(\omega)$ and $SH_0(\omega)$; matrix $[F(\omega)]$ contains transfer functions

$$\begin{bmatrix} R_{SV}(\omega) & R_{SH}(\omega) \\ T_{SV}(\omega) & T_{SH}(\omega) \end{bmatrix}.$$

Approximate expressions for the transfer functions can be obtained by using Figure 4. Incoming S wave in Figure 4 is SV with the vertical incidence and unit amplitude. In anisotropic layer with a horizontal symmetry axis the incoming wave splits into the fast and slow quasi-shear waves. Polarization of the fast wave is parallel to the crystallographic axis a in olivine. Fast direction forms angle β with direction R . Arrows show amplitudes of the incoming and split waves. Amplitudes of the split waves are equal to $\cos\beta$ and $\sin\beta$ for the fast and slow split waves, respectively. Amplitudes of the transfer functions can be obtained by projecting the amplitudes of the split waves on the axes R and T . The resulting expressions for the transfer functions are

$$\begin{aligned} R_{SV}(\omega) &\approx \cos^2 \beta + \sin^2 \beta \exp(-i\omega \delta t), \\ T_{SV}(\omega) &\approx R_{SH}(\omega) \approx -0.5 \sin 2\beta [1 - \exp(-i\omega \delta t)], \\ T_{SH}(\omega) &\approx \sin^2 \beta + \cos^2 \beta \exp(-i\omega \delta t). \end{aligned}$$

Here δt is the traveltime delay of the slow split wave relative to the fast one. Thus, the effect of azimuthal anisotropy can be described by two parameters: (1) fast direction (polarization direction of the fast split wave) and (2) delay of the slow wave relative to the fast one. First parameter is controlled by the direction of symmetry axis in the anisotropic layer. Second parameter is proportional to the strength of anisotropy (difference between the fast and slow velocity) and the thickness of the layer.

Measurements of the parameters of anisotropy beneath the seismograph station are based on the recordings of seismic phase SKS . This phase propagates as the S wave in the mantle and as P wave in the liquid core of the Earth. Due to coupling between SV and P at the core/mantle boundary SKS in isotropic Earth should be polarized as SV . Putting $SH_0(\omega) = 0$ in the expressions for $R(\omega)$ and $T(\omega)$, we get

$$SV_0(\omega) = R(\omega)/R_{SV}(\omega)$$

and

$$T(\omega) = T_{SV}(\omega)R(\omega)/R_{SV}(\omega).$$

Using last expression we can find the theoretical $T(\omega)$ for any pair of the parameters of anisotropy and (by inverse Fourier transformation of $T(\omega)$) the related synthetic seismogram of the T component of SKS phase. The optimum pair provides minimum rms difference between the observed and synthetic T components. This approach has much in common with the receiver function inversion: in both cases one component of wave motion is used to synthesize the other component. In both cases the optimum model minimizes the difference between the observed and synthetic components.

At long periods ($\omega \delta t \ll 1$) the harmonic components of SKS are related as

$$\begin{aligned} R(t) &\approx \cos \omega t, \\ T(t) &\approx 0.5\omega \delta t \sin 2\beta \sin \omega t. \end{aligned}$$

This means that the T component of SKS is shifted in time with respect to the R component by a quarter period, and its amplitude is proportional to frequency. In other words, the T component is proportional to the derivative of the R component. This relation between the R and T components of SKS helps to recognize the effect of azimuthal anisotropy and to distinguish it from lateral heterogeneity. The term $\sin 2\beta$ means that T/R amplitude ratio is a harmonic function of azimuth with a period of π .

Observations of SKS provide excellent lateral resolution but they are insensitive to depth of anisotropy. Distribution of anisotropy with depth can be constrained with the aid of receiver functions. In an isotropic laterally homogeneous Earth, secondary (converted and reflected) phases are polarized strictly in the vertical plane containing the source and the receiver, and their amplitudes are independent of the azimuth. In the presence of azimuthal anisotropy, an appreciable amount of energy of the secondary phases is contained in the T component, and the amplitude of the SV component depends on the azimuth. There are two different mechanisms responsible for the T component of the Ps phases. If this phase is converted from the boundary between two isotropic media, the T component can arise from the splitting of SV . This mechanism is exploited in the SKS techniques. If the phase is converted from the discontinuity between anisotropic media with different anisotropies or from the discontinuity between isotropic and anisotropic media, the T component, like SV , is generated directly by conversion from P . In the process of further propagation, both the SV and T component are modified by shear wave splitting.

Figure 5 demonstrates synthetic seismograms for a medium with azimuthal anisotropy. Anisotropy is hexagonal with a horizontal axis of symmetry. This is the simplest kind of anisotropy that is consistent with the properties of crust and mantle rocks. Anisotropy is in the layer between 30 and 180 km depths, fast direction of anisotropy is 0 degrees, velocities of the fast and slow split waves differ by 3%. Isotropic discontinuity is placed at a depth of 410 km. The only strong wave in the L component is P wave at a time of 0 s. It is followed by arrival at a time of 3 s, which is seen in both H and T components. This phase is formed by conversion from P to S at the upper boundary of the anisotropic layer. Two phases which arrive at a time around 10–12 s are multiple reflections (from the free

surface and the upper boundary of the anisotropic layer). The phases that arrive at a time around 18 s are formed by conversion from P to S at the lower boundary of the anisotropic layer and by subsequent splitting of the S wave in this layer. Finally, the phases that arrive at a time around 40 s are formed by conversion from P to S at a depth of 410 km and splitting of S in the anisotropic layer. There are strong differences between polarities and amplitudes of different phases in the same component and between those of the same phase in different components.

We filtered H and T components of this wavefield in azimuth domain by stacking the traces with weights W_i depending on their azimuths. The weights are different for the Q and T components and are defined as

$$W_i^T(\psi) = \sin 2(\psi - \varphi_i) / \sum_{j=1}^n \sin^2 2(\psi - \varphi_j),$$

$$W_i^Q(\psi) = -\cos 2(\psi - \varphi_i) / \sum_{j=1}^n \cos^2 2(\psi - \varphi_j),$$

where φ is back azimuth of the i -th trace, and ψ is a variable parameter. These filters isolate second azimuthal harmonic with a period of π and introduce a phase shift between the stacks of Q and T components in azimuth domain. The results of azimuthal filtering of traces in Figure 5 are presented in Figure 6. In spite of differences between the initial Q and T components, the stacked traces are remarkably similar. This similarity presents an important criterion to distinguish azimuthal anisotropy from lateral heterogeneity. The actual receiver functions in a broad range of azimuths should be stacked with the azimuth-dependent weights like synthetics in Figure 5. The results of stacking can be inverted for subsurface structure by comparing them with the synthetics that are processed like the actual recordings. The optimum model should also be consistent with the observations of SKS at the same station. This model can be found with a Simulated Annealing algorithm. Examples of analysis of actual data will be demonstrated. The analysis of the secondary phases related to the P wave can be complemented by analysis of precursors to the teleseismic S in various azimuths with the S receiver function technique.

6 Applications of the P and S receiver function techniques

P receiver functions were applied in many regions to map topography of the Moho and other crustal discontinuities. Together with seismic tomography, this is one of the most usable seismic method of regional studies. In a few studies subducting oceanic crust was imaged at a depth reaching 150 km. In other cases, some arrivals can be seen at the times characteristic of the uppermost mantle, but it is usually unclear whether these arrivals are mantle P s phases or crustal reverberations. Another subject which is addressed in a number of studies is topography of the discontinuities bounding the mantle transition zone at depths around 410 km and 660 km. These discontinuities are related to phase transformations with

opposite Clapeyron slopes. Therefore, the differential time between the P660s and P410s phases is sensitive to the mantle temperature: large in the cold regions and small in the hot ones. Indications of hot and cold transition zone are generally found in hotspots and subduction zones, respectively. The hotspot anomalies in a depth range of the transition zone favor the hypothesis of plumes rising from the lower mantle. Some results of mapping the topography of the 410 km and 660 km discontinuities should be viewed with caution, because of large uncertainty in the velocities which are needed for transforming travel times into depths.

S receiver functions were introduced 10 years ago. One of the first successful applications of this method was the analysis of crustal structure of the Moon. Owing to wave scattering, lunar seismograms are very noisy. Coda waves following the arrivals of the *P* wave are comparable in amplitude with the *P* waves, and this makes application of *P* receiver functions impossible. However, in recordings of deep moonquakes there are arrivals of the *S* waves with the amplitudes much larger than the preceding noise. Considerations of the signal/noise ratio favor applications of *S* receiver functions in the future exploration of the Moon and other planets.

On the Earth, low *S* velocity layers were found at those depths, where they were previously either unknown or their presence was doubtful. A low *S* velocity layer was found in several regions at a depth around 500 km; origin of the low velocity might be related to the presence of water in the transition zone. Another well pronounced low *S* velocity layer has been found at a number of locations atop the 410 km discontinuity by using both *P* and *S* receiver functions. This layer is usually found in the regions of mantle upwelling. Its origin can be explained by the difference in solubility of water in the upper mantle (low) and the transition zone (high). If the water concentration in the transition zone is higher than its solubility in the upper mantle, mantle upwelling through the 410-km discontinuity leads to dehydration and melting. Another result of applications of *S* receiver functions is a progress in understanding the Lehmann discontinuity. It is a feature of the continental upper mantle at a depth around 200 km. In the last years this discontinuity was often explained as an effect of a transition from anisotropy in the uppermost mantle to isotropy at depths exceeding 200 km. *S* receiver functions provide arguments against this explanation.

Joint inversion of *P* and *S* receiver functions resulted in a detailed 3-D *S* velocity model of the crust and uppermost mantle of the Tien Shan. The Tien Shan is the largest in the world and most active intracontinental mountain belt. The model provides first plausible explanation for the strange pattern of local seismicity: in the past century large earthquakes occurred only in the peripheral regions, but not in the vast central region. The new model shows that in this region the *S* velocity at depth of 10-35 km is much lower than in adjacent regions. These data are indicative of a mechanical weakness of the crust preventing the accumulation of elastic energy in the central region. The model provides other links between the geodynamics and deep structure of the Tien Shan.

Shear-wave splitting in *SKS* is a subject of many studies. The depth of the observed anisotropy presents a difficult problem of these studies. The joint analysis of *P* receiver functions and *SKS* splitting for seismograph stations in the Tien Shan

has revealed a change in the patterns of azimuthal anisotropy at a depth around 100 km. In the lower layer (asthenosphere), fast directions are aligned with the strike of the belt. This alignment suggests that the anisotropy is an effect of coaxial shortening normal to the strike of the belt. In the upper layer, fast directions are variable. This anisotropy can be a result of thrusting and of ancient deformations.

Intriguing results of joint inversion of P and S receiver functions in southern Africa are a low S velocity atop the 410-km discontinuity and unusually high anelastic attenuation in the upper mantle. These observations, if confirmed, may provide explanation for the Mesozoic-Cenozoic uplift of the Kalahari craton.

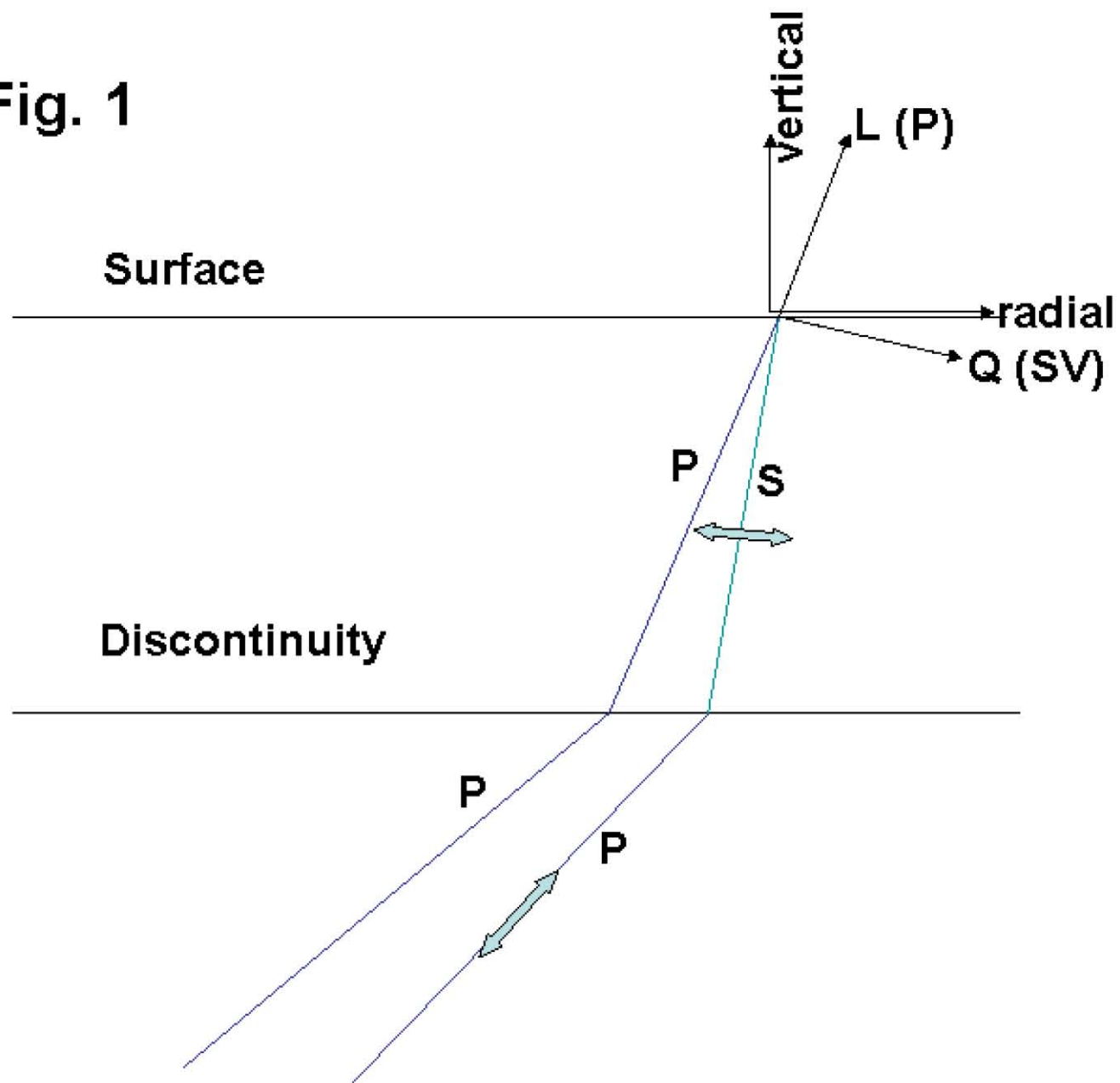
Important observations have been made in India. The Indian shield is mostly Archean. In most other Archean cratons, S velocity in the uppermost mantle is very high (4.7 km/s). This is an effect of a low temperature and a depletion of the upper mantle in the basaltic component. However, beneath the Indian shield seismic velocities at depths less than 200 km are close to the world average (4.5 km/s) which is indicative of either anomalous composition or temperature or both.

References

- [1] Ammon, Ch.J., G.E. Randall, and G. Zandt, On the nonuniqueness of receiver function inversions, *J. Geophys. Res.*, 95, 15303-15318, 1990.
- [2] Berkhout, A.J. Least square inverse filtering and wavelet deconvolution, *Geophysics*, 42, 1369-1383, 1977.
- [3] Bostock, M., Green's functions, source signatures, and the the normalization of teleseismic wave fields, *J. Geophys. Res.*, 109, doi:10.1029/2003JB002783.
- [4] Cassidy, J.F., Numerical experiments in broadband receiver function analysis, *Bull. Seism. Soc. Am.*, 67, 677-691, 1992.
- [5] Dueker, K. G., and A. F. Sheehan, Mantle discontinuity structure from mid-point stacks of converted P to S waves across the Yellowstone hotspot track, *J. Geophys. Res.*, 102, 8313-8327, 1997.
- [6] Farra, V., and L. Vinnik, Upper mantle stratification by P and S receiver functions, *Geophys. J. Int.*, 141, 699-712, 2000.
- [7] Flanagan, M., and P. Shearer, Global mapping of topography on transition zone velocity discontinuities by stacking SS precursors, *J. Geophys. Res.*, 103, 2673-2692, 1998.
- [8] Haskell, N.A., Crustal reflection of plane P and SV waves, *J. Geophys. Res.*, 67, 4751-4767, 1962.
- [9] Jasbinsek, J. and K. Dueker, Ubiquitous low-velocity layer atop the 410-km discontinuity in the northern Rocky Mountains. *Geochem.Geophys.Geosys.*8(101):doi:10.1029/2007GC001661.
- [10] Kanasevich, R. E., C.D. Hemmings, and T. Alpaslan, N-th root stack non-linear multichannel filter, *Geophysics*, 38, 327-338, 1973.
- [11] Keith, C. M. and S. Crampin, Seismic body waves in anisotropic media: Propagation through a layer, *Geophys. J. R. astr. Soc.*, 49, 209-223, 1977.
- [12] Langston, C. A., Structure under mount Rainier, Washington, inferred from teleseismic body waves, *J. Geophys. Res.*, 84, 4749-4762, 1979.
- [13] Mosegaard, K. and M. Sambridge, Monte Carlo analysis of inverse problems, *Inverse problems*, 18, 29-54, 2002.
- [14] Petersen, N., and L. Vinnik, Detection of crustal converted phases as a problem of multichannel filtering, *Proc. Acad. Sci. Russ., Physics of the Earth*, 4, 37-44, 1991 (in Russian).
- [15] Revenaugh, J., and T.H. Jordan, A study of mantle layering beneath the Western Pacific, *J. Geophys. Res.*, 94, 5787-5813, 1989.

- [16] Silveira, G., L. Vinnik, E. Stutzmann, V. Farra, S. Kiselev, I. Morais, Stratification of the Earth beneath the Azores from P and S receiver functions, *Earth Planet. Sci. Lett.*, 2010 (in press).
- [17] Vinnik, L.P., Detection of waves converted from P to SV in the mantle, *Phys. Earth Planet. Inter.*, 15, 39-45, 1977.
- [18] Vinnik, L.P., G.L. Kosarev, and L.I. Makeyeva, Lithospheric anisotropy as indicated by SKS and SKKS waves, *Doklady - Earth Sci. Sections*, 278, 39-43 (published in English by Scripta Technica), 1984.
- [19] Vinnik, L., S. Oreshin, G. Kosarev, S. Kiselev and L. Makeyeva, Mantle anomalies beneath southern Africa: Evidence from seismic S and P receiver functions, *Geophys. J. Int.*, 179(1), 279-298, 2009.
- Vinnik, L., Y. Ren, E. Stutzmann, V. Farra and S. Kiselev, Observations of $S410p$ and $S350p$ phases at seismograph stations in California, *J. Geophys. Res.*, 115, doi:10.1029/2009JB006582, 2010.
- [20] Zhao, L.-S., M. K. Sen, P. Stoffa, C. Frolich, Application of very fast simulated annealing to the determination of the crustal structure beneath Tibet, *Geophys. J. Int.*, 125, 355-370, 1996.
- [21] Zhu, L., H. Kanamory, Moho depth variations in southern California from teleseismic receiver functions, *J. Geophys. Res.*, 105, 2969-2980, 2000.

Fig. 1



Axes are rotated from vertical and radial to L, Q. L is parallel to the principal motion direction in the P wave.

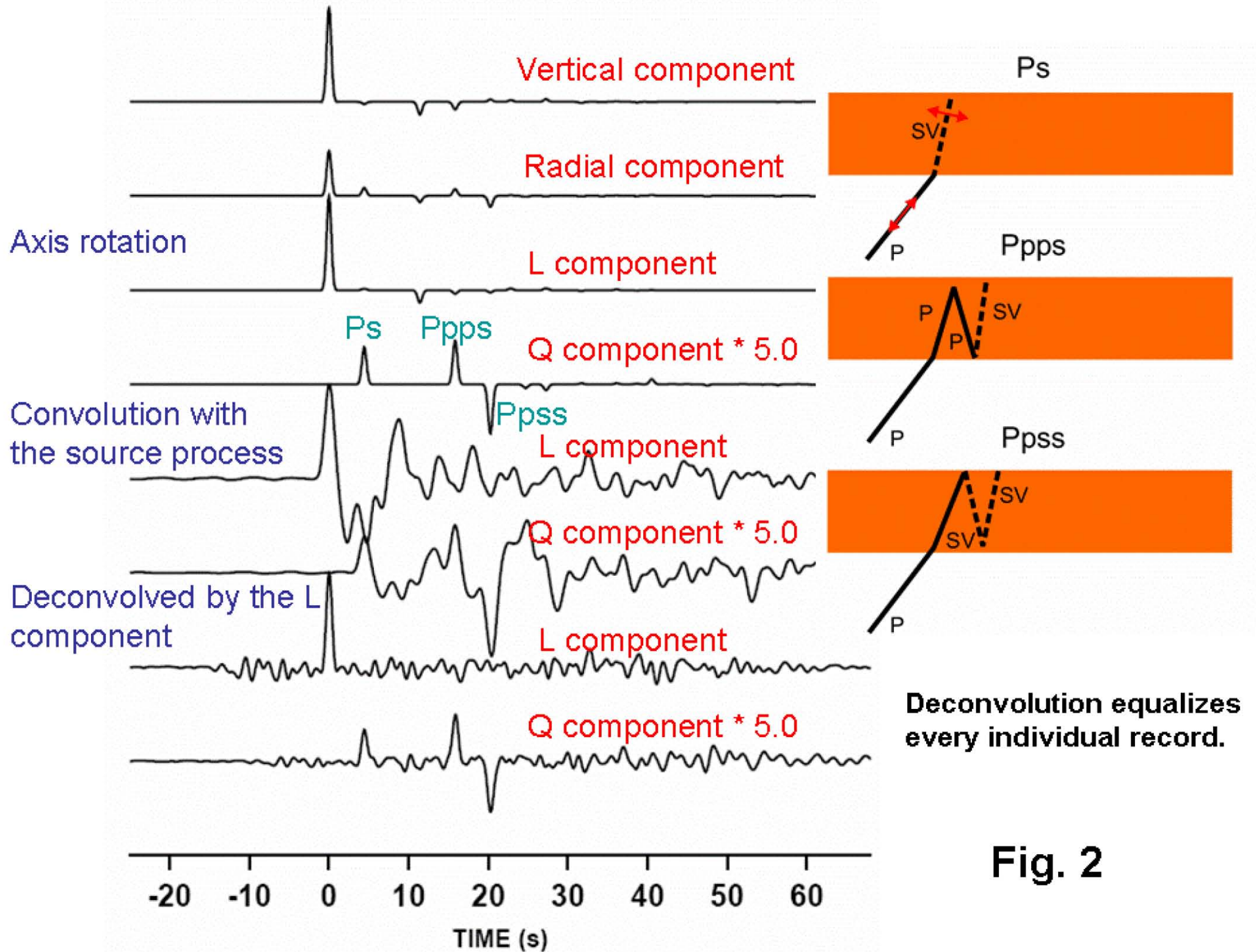
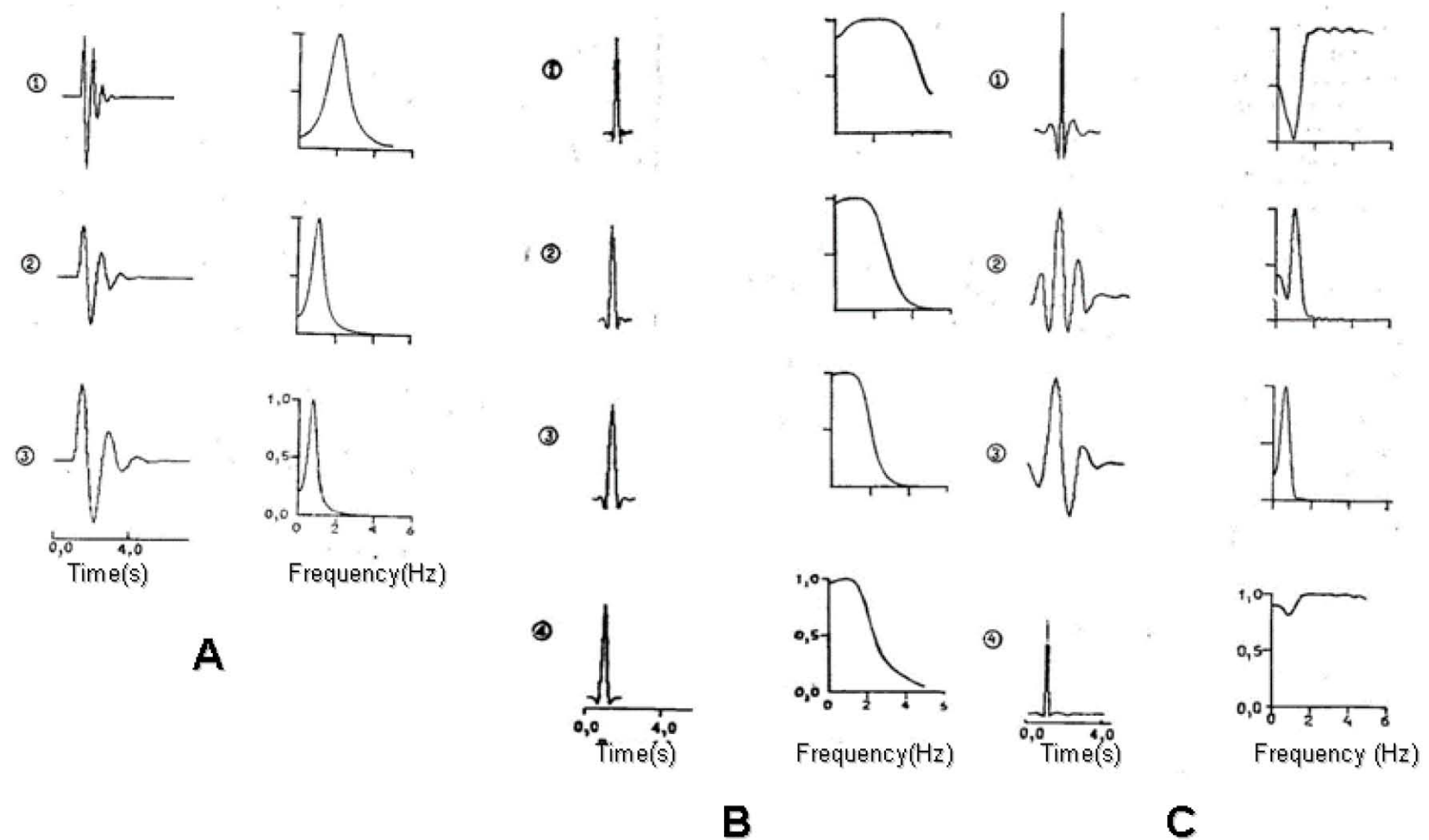


Fig. 2



Example of multi-channel deconvolution. A – three waveforms and their amplitude spectra; B – single-channel deconvolution (1-3) and stack (4); C - multi-channel deconvolution (1-3) and stack (4).

Fig. 3

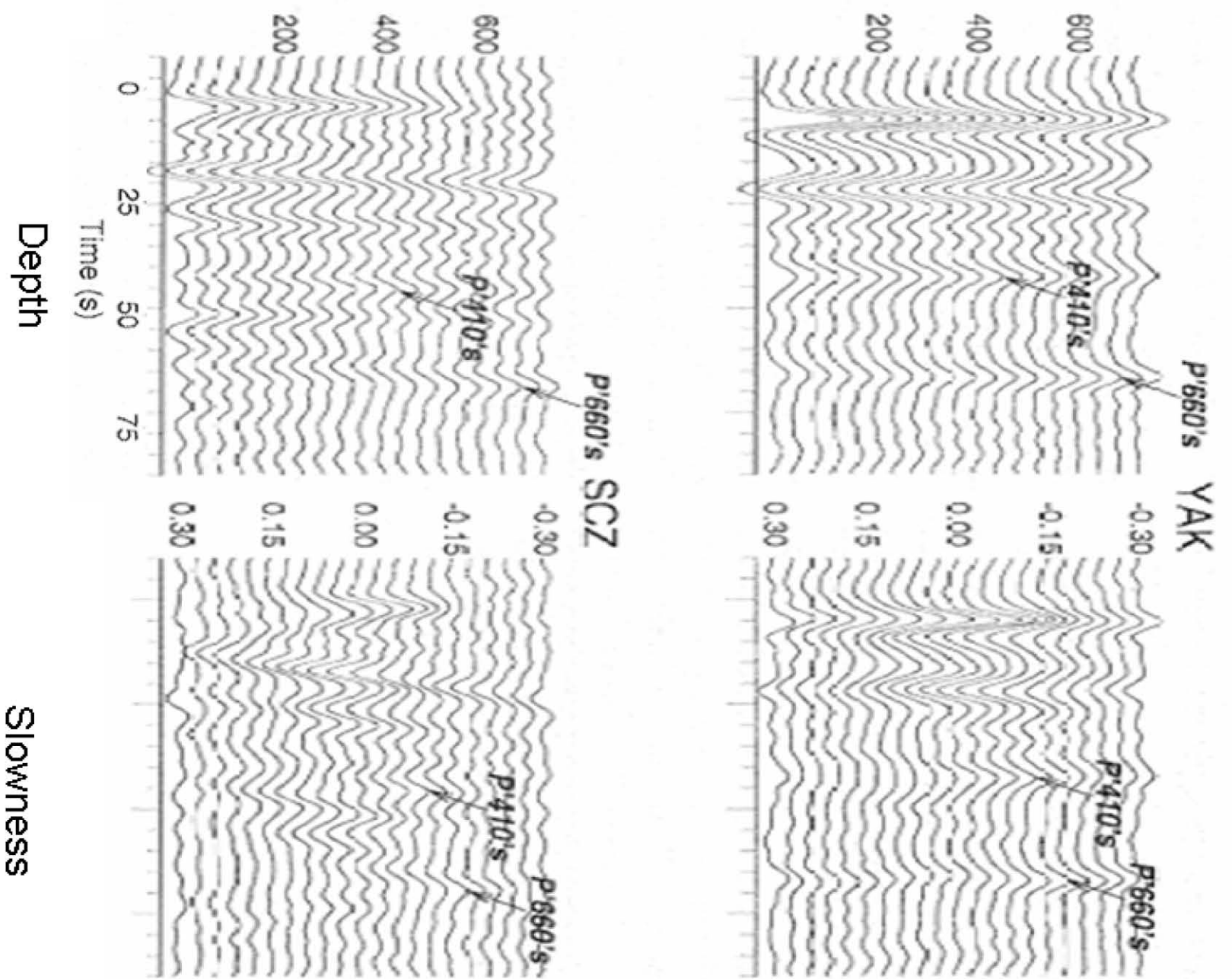
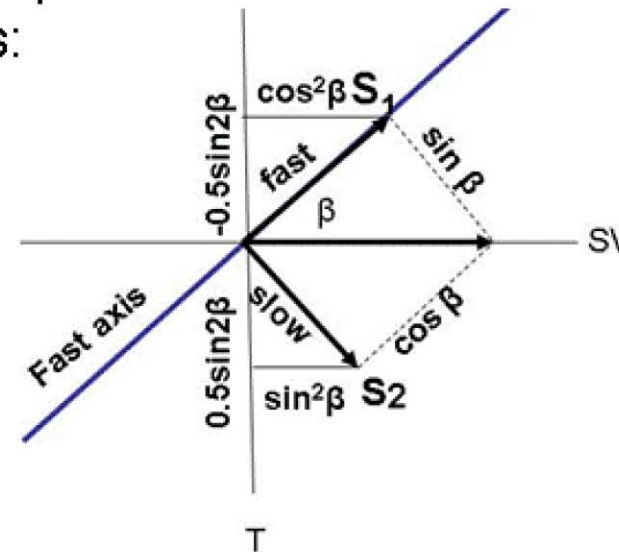


Fig. 4

$$\begin{vmatrix} R(\omega) \\ T(\omega) \end{vmatrix} = \begin{vmatrix} R_{SV}(\omega) & R_{SH}(\omega) \\ T_{SV}(\omega) & T_{SH}(\omega) \end{vmatrix} \begin{vmatrix} SV_0(\omega) \\ SH_0(\omega) \end{vmatrix}$$

For vertical propagation, approximate expressions for the transfer functions can be obtained by using geometrical relations:



Arrows show amplitudes and polarizations of the incoming and split waves. Incoming S wave is SV with vertical incidence and unit amplitude. Amplitudes for the T components of the fast and slow split waves are $-0.5 \sin 2\beta$ and $0.5 \sin 2\beta$. Amplitudes of the R components are $\cos^2(\beta)$ and $\sin^2(\beta)$. The slow wave arrives with a delay δt . The resulting expression for the transfer functions are:

$$\begin{aligned} R_{SV}(\omega) &\approx \cos^2 \beta + \sin^2 \beta \exp(-i\omega \delta t), \\ T_{SV}(\omega) &\approx R_{SH}(\omega) \approx -0.5 \sin 2\beta [1 - \exp(-i\omega \delta t)], \\ T_{SH}(\omega) &\approx \sin^2 \beta + \cos^2 \beta \exp(-i\omega \delta t). \end{aligned}$$

Fig. 5

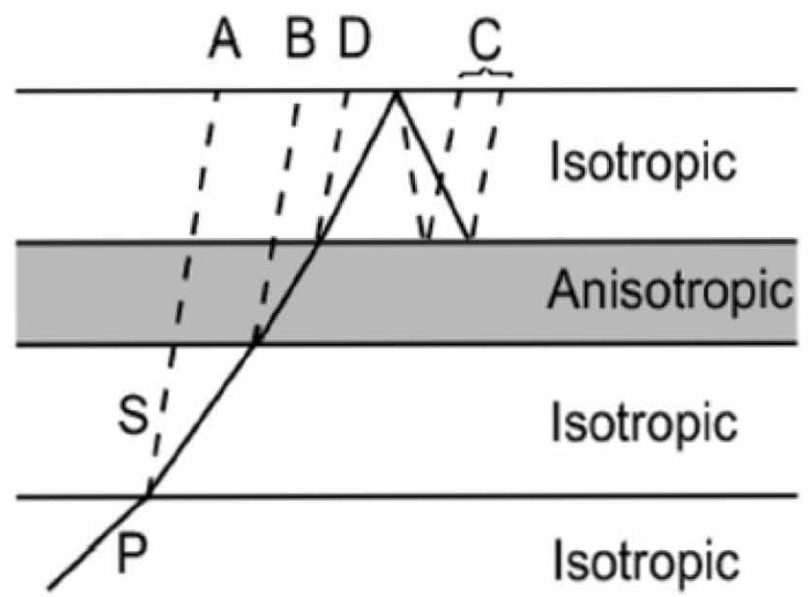
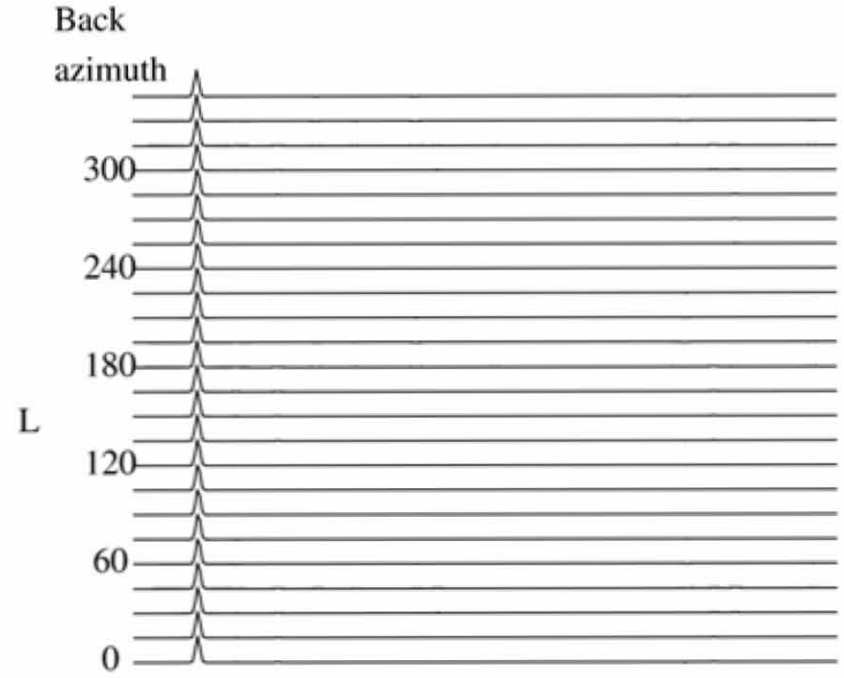
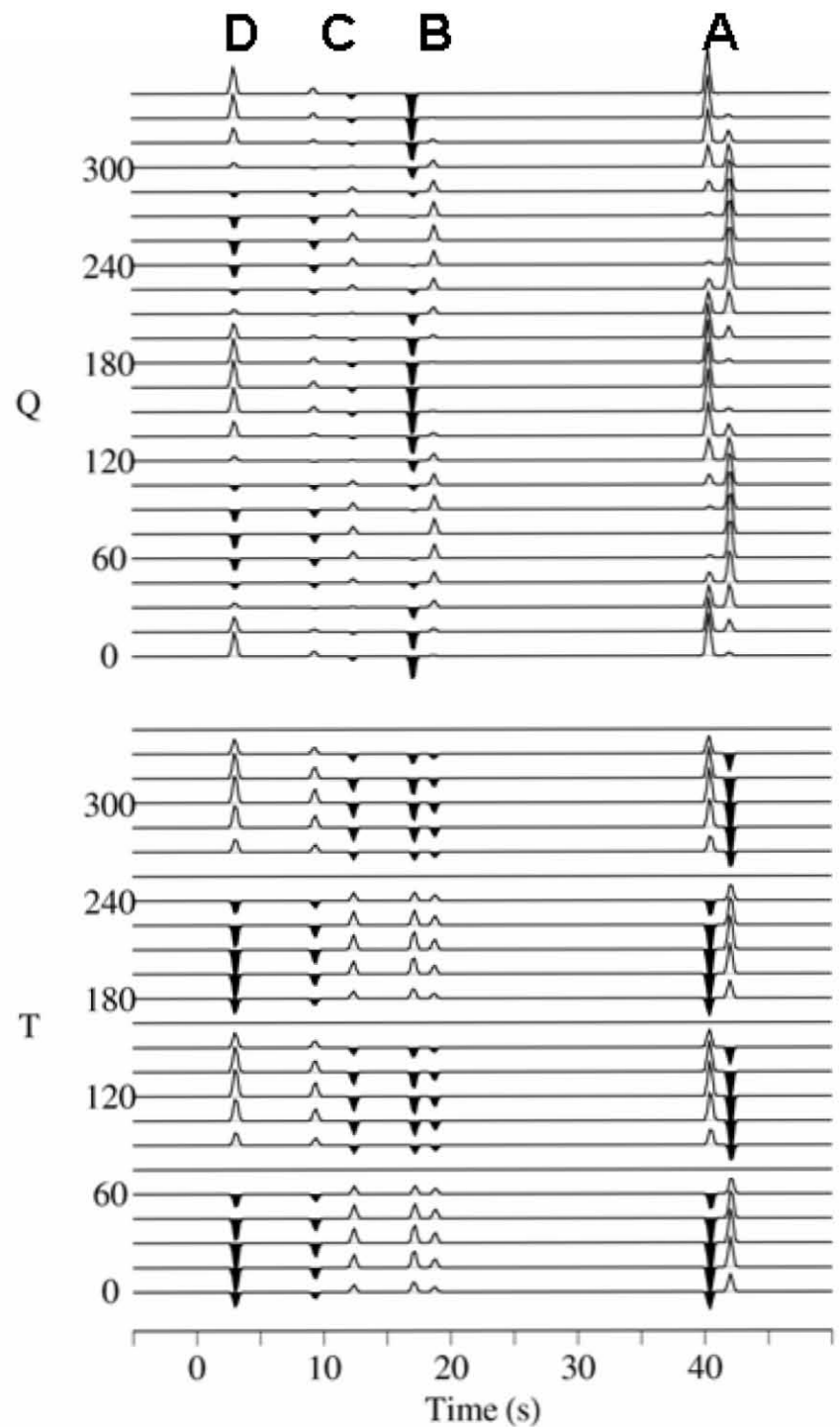


Fig. 6

We assume that the receiver functions are obtained for discrete values φ_i of back azimuth with a small sampling interval in the range from 0 to 360°. Horizontal components of the receiver function with the azimuth of φ_i are $Q_i(t)$ and $T_i(t)$. For these components we define weighting coefficients $W_i^Q(\psi)$ and $W_i^T(\psi)$:

$$W_i^Q(\psi) = -\cos 2(\psi - \varphi_i) / \sum_i \cos^2 2(\psi - \varphi_i)$$

$$W_i^T(\psi) = \sin 2(\psi - \varphi_i) / \sum_i \sin^2 2(\psi - \varphi_i)$$

The components of the receiver functions are stacked with weights:

$$QF(t, \psi) = \sum_i W_i^Q(\psi) Q_i(t)$$

$$TF(t, \psi) = \sum_i W_i^T(\psi) T_i(t)$$

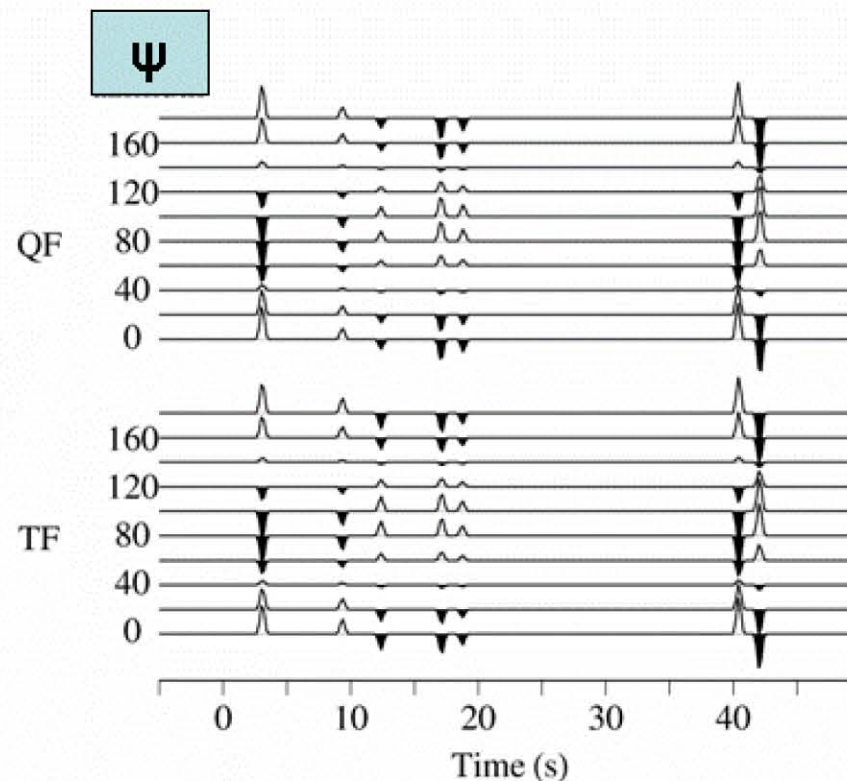


Fig. 7